Materials Advances

ROYAL SOCIETY OF CHEMISTRY

PAPER

View Article Online
View Journal | View Issue

Cite this: DOI: 10.1039/d3ma01062g

Eco-friendly repurposing of by-pass waste for optics and radiation protection: addressing hazardous material challenges

Hesham M. H. Zakaly, *[ab] H. Hashim,[c] Shams A. M. Issa,[bd] Moustafa A. Darwish,*[c] Fatma M. Obiedallah,[e] M. S. I. Koubisy[a] and H. A. Saudi[f]

This study delves into the investigation of optical and gamma radiation shielding properties of glasses formulated with varying concentrations of By-pass combined with Na_2O, Fe_2O_3, Bi_2O_3, and P_2O_5. The specific compositions were represented as ((*x*) By-pass–(20) Na_2O–(10) Fe_2O_3–(20) Bi_2O_3–(50–*x*) P_2O_5), with "*x*" ranging from 0 to 15 wt%. The structural and optical properties of these glasses were rigorously analyzed using X-ray diffraction (XRD), UV-visible spectroscopy, and other characterization techniques, revealing the absence of Bragg peaks and highlighting the amorphous nature of the samples. Notably, increasing By-pass concentration enhanced UV-visible absorption, particularly in the 400 nm to 850 nm range. Radiation shielding assessments were conducted across photon energies ranging from 80 to 2614 keV. The results highlighted that the linear and mass attenuation coefficients were inversely proportional to the photon energy. The By-pass15 glass, with the highest By-pass concentration, consistently demonstrated superior shielding attributes compared to its counterparts, with the lowest half-value layer (G_{HVL}) values and the most substantial radiation protection efficiency (RPE). Comparative assessments with other glasses and concrete types further accentuated the potential of the By-pass15 glass as a promising candidate for gamma radiation shielding applications. In conclusion, this research paves the way for potentially utilizing By-pass15 glass in environments where radiation protection is imperative. Incorporating By-pass in glass composites enhances their gamma shielding efficiency and promotes the sustainable use of By-pass, underscoring the dual advantages of this innovative approach.

Received 29th November 2023,
Accepted 15th February 2024

DOI: 10.1039/d3ma01062g

rsc.li/materials-advances

1. Introduction

Environmental preservation is an imperative responsibility for the global community in the current era. The escalating concerns about ecological degradation, driven largely by improper disposal of industrial wastes and the proliferation of harmful materials, have called for innovative strategies to transform potential pollutants into beneficial products. This eco-conscious shift from waste generation to sustainable utilization is not just about conservation; it's about ushering in a new epoch of sustainable development.[1,2] One such promising avenue is the transformation of harmful industrial by-products into high-value materials with exceptional properties. Glass, an ancient material with diverse applications, presents a unique opportunity. Traditionally valued for its transparency and malleability, recent advancements have expanded its utility to optics and radiation shielding realms. Modern glass formulations doped with specific elements or compounds can exhibit remarkable optical characteristics, making them indispensable in advanced technological applications ranging from opto-electronics to photonics.[3–6]

Radioactive isotopes and related technologies significantly influence modern human life. Naturally occurring isotopes serve as a source of radiation with various applications. Their detectable radioactivity makes them ideal tracers. They can also eliminate harmful agents from food due to the energy they emit. Moreover, isotopes have diverse medical roles, such as using radioactive ^{131}I to assess thyroid functionality.[7,8] Yet, unintended radiation exposure from these isotopes can harm living organisms and the environment. The potential harm

[a] Faculty of Science, Al-Azhar University, Assiut Branch, Assiut 71524, Egypt. E-mail: h.m.zakaly@gmail.com
[b] Institute of Physics and Technology, Ural Federal University, Yekaterinburg 620002, Russia
[c] Physics Department, Faculty of Science, Tanta University, Tanta 31527, Egypt. E-mail: mostafa_ph@science.tanta.edu.eg
[d] Physics Department, Faculty of Science, University of Tabuk, Tabuk 71451, Saudi Arabia
[e] Physics Department, Faculty of Science, Assiut University, Assiut 71516, Egypt
[f] Physics Department, Faculty of Science (Girls Branch), Al-Azhar University, Egypt

depends on the type and amount of energy they release. For example, high doses can lead to conditions like cataracts, DNA damage, infertility, and several diseases.[9] Thus, those handling radioactive materials are advised to use shielding materials to minimize exposure risks.[10–12] Historically, due to their high atomic numbers and density, materials like lead, concrete, and lead composite have been favored for nuclear safety applications. However, concerns like toxicity have limited the use of lead products.[13] This has prompted the search for alternative materials. In this quest, glass systems emerge as potential candidates. They offer advantages over other materials, such as cost-effectiveness, ease of fabrication, recyclability, and light transparency.[14] Specifically, glasses infused with heavy metal oxides, like Bi_2O_3, are gaining traction. Their high density and unique features make them apt for radiation shielding tasks.[15–18]

In recent years, exploring silicate structural, optical, and radiation shielding properties of studies such as the innovative doping of soda-lime-silica glasses with organic compounds like peanut shell powder have opened new avenues for modifying optical properties while promoting sustainability.[19] Further investigations, as documented,[20,21] have delved into the complex interplay between glass composition and its impact on light transmission and radiation protection efficiency. Recent work highlighted[18] has also contributed to our understanding of the structural characteristics crucial for developing non-toxic, eco-friendly radiation shielding materials. These studies underscore the importance of continuous innovation in glass science, particularly in leveraging various dopants and waste materials, to achieve enhanced performance in optical applications and radiation shielding.[22–25]

This research examines the usefulness of prepared glasses in shielding applications at different photon energies. The primary focus of the current study is to experimentally investigate the radiation attenuation characteristics of By-pass glasses, which comprise SiO_2, Al_2O_3, Fe_2O_3, TiO_2, CaO, MgO, Na_2O, and K_2O (as a modifier). For gamma the effect of systematically replacing By-pass with P_2O_5 on the attenuation characteristics was dissected in great depth. This study also gives a wide-scope comparison of the shielding performance of the current recommended system compared with the typically employed systems. The selection of By-pass waste as a primary material in the present study was driven by multiple factors. First and foremost, By-pass waste, a by-product of the cement industry, poses significant environmental challenges due to its large volume generation and disposal issues.[26–28] Its composition, rich in silica and alumina, alongside other oxides such as calcium oxide and iron oxide, makes it a potential candidate for glass synthesis, leveraging its waste-to-wealth conversion potential.[29,30] Furthermore, incorporating By-pass waste into glass composites aligns with global efforts towards sustainable development by reducing landfill use and promoting the recycling of industrial by-products.[31] Additionally, previous studies have indicated that certain waste materials can enhance glasses' optical and radiation-shielding properties. Therefore, By-pass waste was selected to investigate its efficacy in improving these properties while addressing environmental conservation and waste management challenges. Beyond optics, there's an emergent demand for materials that can shield against harmful radiation, especially in medical, industrial, and nuclear domains. With the growing reliance on nuclear energy and medical radiation, ensuring safety has become paramount. Herein lies the novelty of re-engineering harmful by-products into specialized glass composites that can attenuate harmful radiations. Such advancements address the pressing issue of waste management and provide solutions to critical challenges in radiation protection.

In essence, the convergence of environmental protection with the creation of high-performance materials represents a pioneering approach. It signifies the dawning of an era where harmful residues are no longer discarded but are transformed, through the alchemy of science and innovation, into materials that protect, serve, and inspire. This research underscores the importance and potential of such transformations, highlighting the dual benefits: safeguarding our environment while meeting the demands of cutting-edge technological applications.

2. Materials and methods

2.1. Sample preparation

Cement dust, characterized as By-pass, was sourced from cement factories located in Beni Suef (Egypt). Recognized as industrial waste, this waste (dust) was first analyzed using X-ray fluorescence (XRF) to determine its chemical composition. The predominant elements in the By-pass included 47.67% SiO_2, 4.24% Al_2O_3, 2.14% Fe_2O_3, 0.20% TiO_2, 37.95% CaO, 3% MgO, 2.95% Na_2O, and 1.85% K_2O, cumulatively accounting for 100% of its total oxide content.

To synthesize the glass samples, five distinct concentrations of the By-pass mixture were prepared, adhering to the composition formula ((x) By-pass–(20) Na_2O–(10) Fe_2O_3–(20) Bi_2O_3–(50–x) P_2O_5), where "x" ranged from 0 to 15 wt%. The mixtures were stirred continuously at room temperature to ensure homogeneity. Once mixed, the samples were placed in an oven preheated to 1450 °C and melted for two hours. Following the melting, the hot molten samples were carefully poured onto a stainless-steel bar to shape them. The steel bar, now containing the samples, was then transferred to a secondary furnace set at 300 °C. The samples were annealed at this temperature and subsequently cooled down gradually to room temperature. This two-step thermal process ensured the prepared glass samples' structural integrity and amorphous nature.

2.2. Characterizations and measurements

The narrow beam approach, combined with a lead-collimator, was utilized to acquire experimentally established linear attenuation coefficients (G_{LAC}). The values were acquired using a NaI(Tl) scintillation detector with a measuring area of 3 inches by 3 inches and coupled to a multichannel analyzer. Throughout the experiment, the following radioactive sources were utilized: ^{133}Ba (5 μCi, 80 keV), ^{137}Cs (5 μCi, 662 keV), ^{60}Co (10 μCi, 1173 and 1333 keV), and ^{232}Th (20 μCi, 238, 911, and

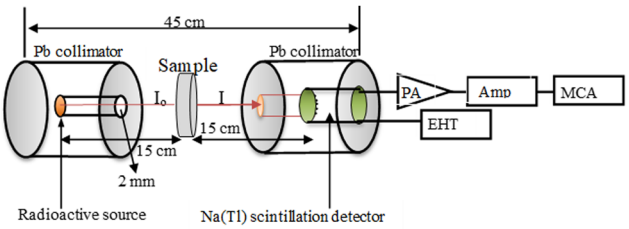

Fig. 1 Experimental radiation measurement setup.

2614 keV). Fig. 1 illustrates the experimental setup, which includes the source, the sample, and the detector in their appropriate locations. Calculations were performed to estimate the photon intensity without and with the absorber for each gamma line using the region underneath the photopeak. These calculations were essential to determine the photon intensity.

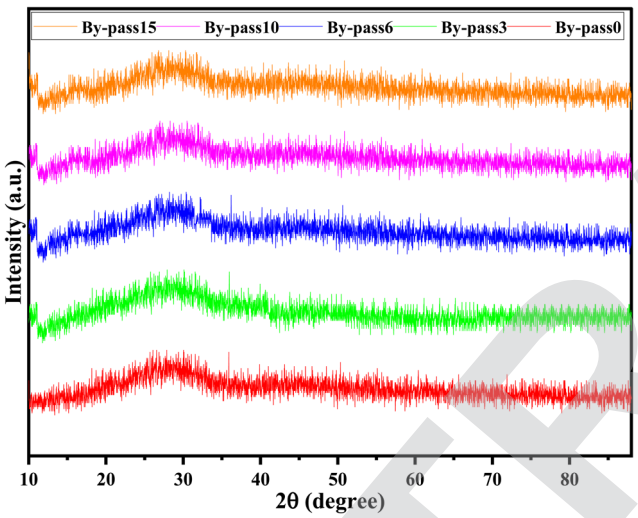

Fig. 2 XRD patterns of the prepared samples.

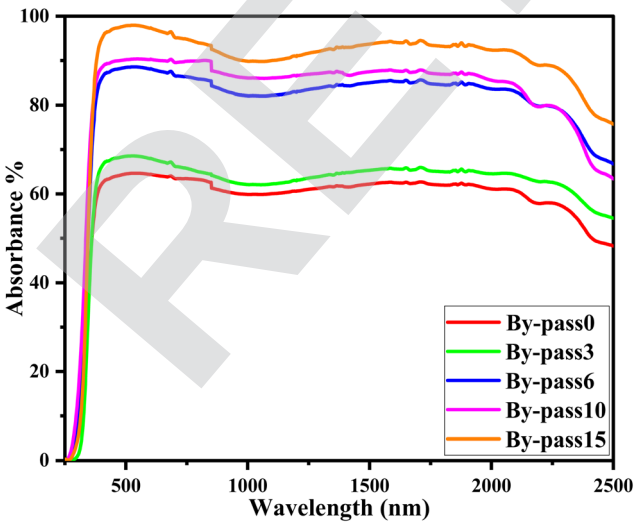

Fig. 3 UV-visible absorption profiles of the prepared samples.

The process was repeated five times, and 10 minutes were set aside for each iteration of the method. The level of uncertainty was far lower than one percent.

3. Results and discussion

3.1. XRD analysis

By-pass and transparent glasses were synthesized using the composition ((*x*) By-pass-(20) Na_2O–(10) Fe_2O_3–(20) Bi_2O_3–(50–*x*) P_2O_5), where *x* = 0 (By-pass0), 3 (By-pass3), 6 (By-pass6), 10 (By-pass10), and 15 (By-pass15) wt% through the conventional melt quenching technique. The XRD patterns of the various By-pass glass samples exhibited remarkable similarity, characterized by the absence of Bragg peaks, as illustrated in Fig. 2. This absence of peaks confirms the amorphous nature of the glassy phase of the samples, where the amorphous regions would contribute a broad, low-intensity background. Additionally, no discernible peak corresponding to By-pass was observed, which reveals that the added quantity of By-pass has been fully incorporated into the glass matrix.[32,33]

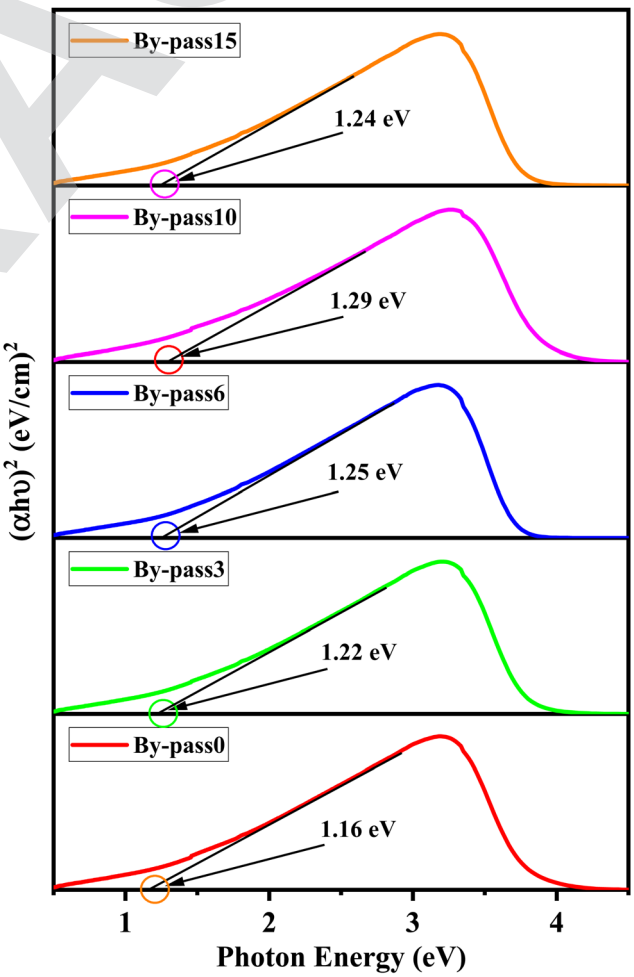

Fig. 4 Estimated indirect band gap for different By-pass concentrations employing Tauc's equations.

Table 1 The direct and indirect band gaps for the composite at different concentrations of By-pass (x)

x (wt%)	Direct band gap (eV)
0	1.16
3	1.22
6	1.25
10	1.29
15	1.24

3.2. Optical properties

3.2.1. UV-visible spectroscopy analysis. UV-visible spectroscopy was performed using a UV-visible spectrometer, focusing on samples with a thickness of 0.43 cm. The spectra were scanned across the wavelength range of 250 to 2500 nm, as illustrated in Fig. 3. Analysis of the UV-visible absorption spectra revealed a significant increase in absorption values, specifically between 400 nm and 850 nm, as the concentration of By-pass in the composite is progressively increased. This observation strongly supports the notion that including By-pass markedly enhances the absorption capacity of the composite. This enhancement is attributed to the incident photon beam possessing sufficient energy to facilitate electron transfer from the valence band to the conduction band, with the remainder of the photon energy being absorbed by the samples. Notably, this effect is most pronounced in the By-pass15 sample, which boasts the highest By-pass concentration and consistently exhibits superior absorption compared to the other samples. However, as we shift to higher wavelengths, the peak positions remain remarkably consistent across all concentrations, signifying the unaltered nature of the electronic transitions.

Nevertheless, there is a slight variation in the intensity of these peaks associated with changing concentration. As we approach the wavelength range of 2100 nm to 2500 nm, the incident photon beam carries lower energy, reducing interactions with atomic structures within the composite. This suggests that By-pass plays a crucial role in enhancing the light–material interaction in the composite. Consequently, the composite featuring the highest By-pass concentration demonstrates the most robust interactions with UV-visible light among all the samples examined.

3.2.2. Bandgap energy. Determining the band gap of a material from its UV-visible absorption data involves plotting the transformed data to reveal the band gap as an intercept on the x-axis.

The Tauc plot is commonly used for this purpose. First, we need to approximate the absorption coefficient (α) from the absorption data using eqn (1):[34]

$$\alpha = \frac{2.303 \times A}{t} \quad (1)$$

where (A) is the absorbance, and (t) is the thickness of the glass sample in (cm), in our work, t = 0.43 cm. The Tauc relationship is given by eqn (2):[35,36]

$$(\alpha h\nu)^n = A(h\nu - E_g) \quad (2)$$

where ($h\nu$) is the photon energy which can be calculated as ($1240/\lambda$), where 1240 is a constant in eV and (λ) is the wavelength in nm, (E_g) is the optical band gap, (A) is a constant, and n = 2 for indirect transition and $n = \frac{1}{2}$ for direct transition.

To determine the indirect transition band gap, we can plot ($(\alpha h\nu)^2$) *vs.* ($h\nu$). The direct optical band gap values are determined by identifying the intercepts where the linear portion of the curve extrapolates to meet the linear axis representing

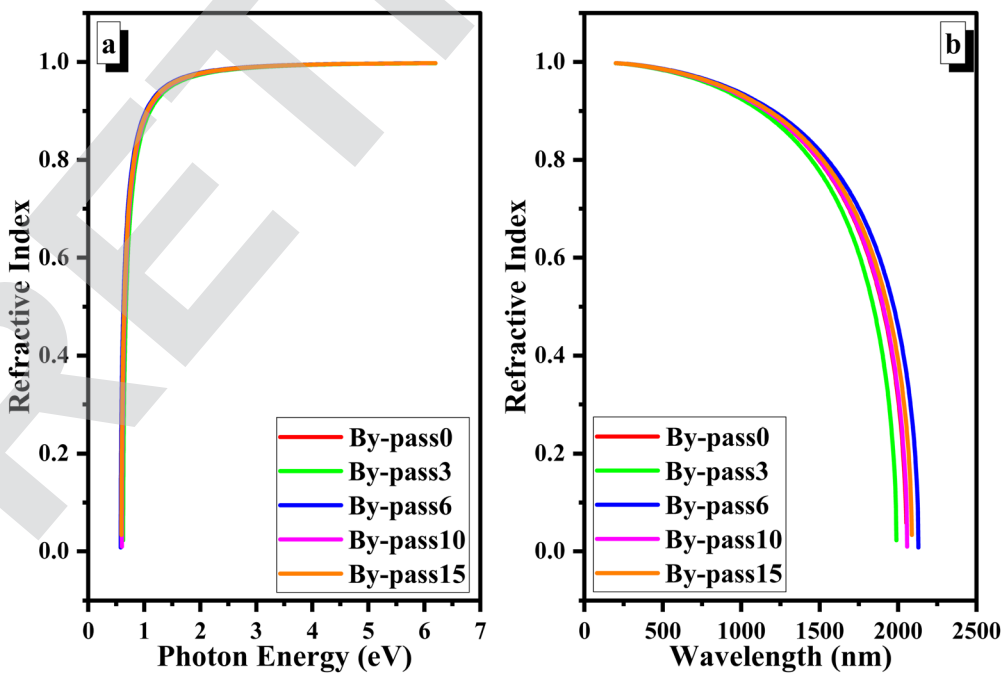

Fig. 5 The refractive index against photon energy (a) and the wavelength (b) for different concentrations of By-pass in the studied samples.

photon energy. Fig. 4 shows that as the By-pass concentration increases from 0 to 15 wt%, the optical band gap energy increases from 1.16 to 1.29 eV, as tabulated in Table 1. This increase implies that adding By-pass atoms to glass fabricates new energy levels in the band gap. These new energy levels act as traps for valence electrons, making the transition to high energy states in the conduction band more difficult.[37]

3.2.3. Refractive index. The refractive index (n) is a fundamental property of materials, indicating how much light is refracted as it passes through the material and can be determined from transmittance data, which can be calculated from absorbance data using eqn (3):[38]

$$T = 10^{(-A)} \times 100 \quad (3)$$

The relationship of refractive index is given by eqn (4):[39]

$$n^2 = \frac{1}{T-1} + \frac{1}{T} \quad (4)$$

where (T) is the percentage transmission coefficient.

Fig. 5(a) shows the refractive index variation *versus* photon energy. At low photon energies, the refractive index increases with increasing photon energy. While at high photon energies, it exhibits a plateau. This is likely due to changes in the electronic structure and density resulting from different By-pass concentrations. The variation in the refractive index across different By-pass concentrations indicates that the optical properties of the composite are sensitive to the By-pass content, particularly at low photon energies. Fig. 5(b) shows that the wavelength increases the refractive index and shows a general decreasing trend due to increased transmittance and decreased absorption of traps and intraband transitions across different concentrations of By-pass.

3.2.4. Extinction coefficient. The extinction coefficient, often represented by (k), measures the amount of absorption loss when light passes through a material. It's closely related to the absorption coefficient (α) and provides insights into how efficiently a material can absorb light at a specific wavelength or photon energy. The relationship between the absorption coefficient (α) and the extinction coefficient (k) is given by eqn (5):[40]

$$k = \frac{\alpha\lambda}{4\pi} \quad (5)$$

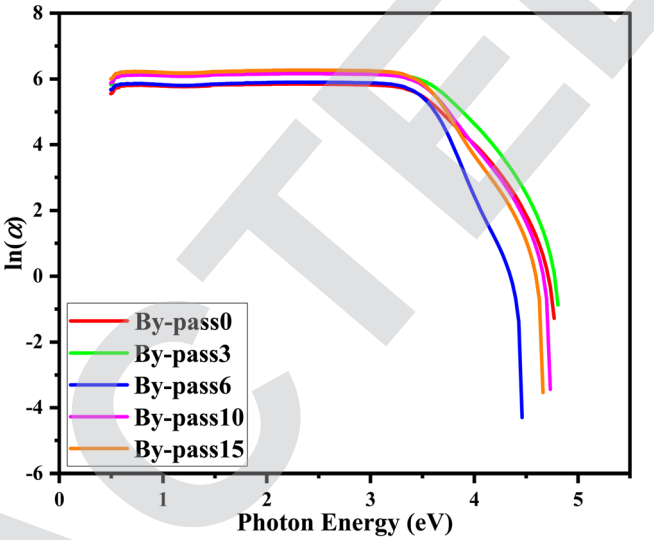

Fig. 7 The relationship between (ln(α)) and photon energy for different concentrations of By-pass in the studied samples.

Table 2 The Urbach energies (E_U) for the composite's different concentrations of By-pass (x)

x (wt%)	E_U (eV)
0	~2.77
3	~3.05
6	~2.31
10	~2.49
15	~2.35

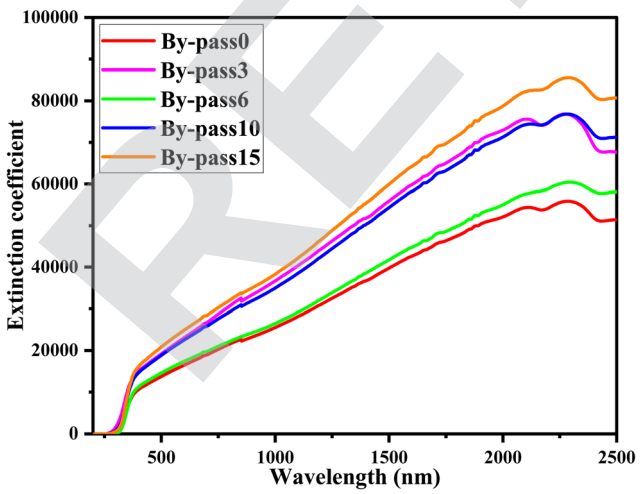

Fig. 6 The extinction coefficient against the wavelength for different concentrations of By-pass in the studied samples.

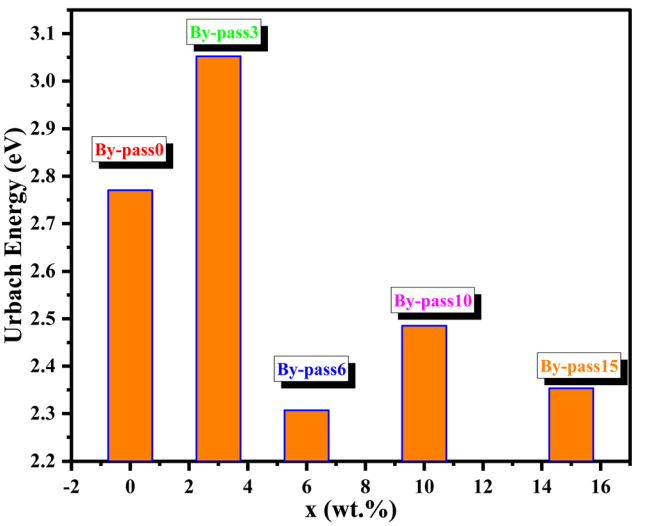

Fig. 8 The Urbach energy for different concentrations of By-pass (x) in the studied samples.

where (α) is the absorption coefficient, which we have previously determined, and (λ) is the wavelength of light. Using eqn (5), the extinction coefficient (k) can be computed for each wavelength and different concentrations of By-pass in the composite. Fig. 6 shows the extinction coefficient (k) as a function of wavelength and By-pass concentration. The extinction coefficient increases with wavelength, which implies that the glass absorbs and scatters more light at longer wavelengths. The effective wavelength around 2300 nm is the wavelength at which the extinction coefficient is highest. This means the glass absorbs and scatters most of the incident light at this wavelength.[41]

3.2.5. Urbach energy. The Urbach energy, often denoted as (E_U), measures the width of the band tail states in disordered materials. These band-tail states arise due to disorder and local potential fluctuations in the material, leading to a non-zero density of states in the energy gap of a semiconductor. Urbach energy is important as it provides insights into the degree of disorder in the material. The absorption coefficient (α) near the band edge of

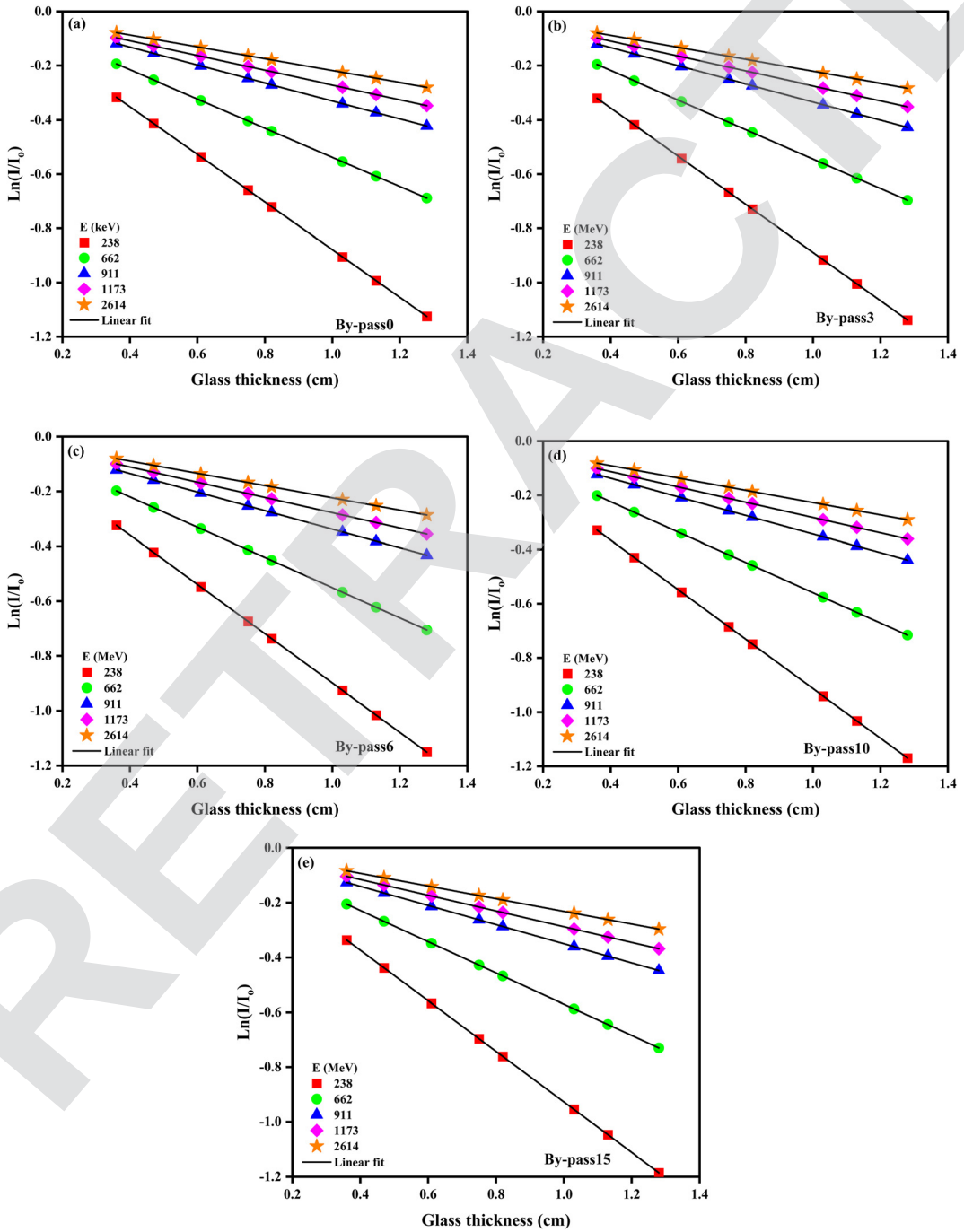

Fig. 9 (a)–(e) Transmission factor (Ln(I/I_0)) against glass thickness at selected photon energy.

disordered materials can be described by the Urbach rule, eqn (6):[42]

$$\alpha(E) = \alpha_0 \exp\left(\frac{E}{E_U}\right) \quad (6)$$

where ($\alpha(E)$) is the absorption coefficient at photon energy (E), and (α_0) is a constant. From eqn (10), (E_U) can be determined by plotting ($\ln(\alpha)$) *versus* (E) and extracting the reciprocal of the slope. The steeper the slope, the greater the disorder in the material.

The Urbach energy provides insights into the degree of disorder in a material. A larger Urbach energy typically indicates a higher degree of disorder or structural imperfections in the material. However, it appears that there are regions where (α) is zero or very close to zero, leading to undefined values in ($\ln(\alpha)$), as shown in Fig. 7. This has affected our ability to extract the Urbach energy directly from the graph. If we could extract the Urbach energy, variations across different concentrations would provide insights into how By-pass affects the disorder in the composite. We focused on a photon energy range where (α) values are non-zero and well-defined to ensure accurate linear fits and determination of the Urbach energy. By-pass may introduce or alleviate certain structural or electronic irregularities, manifesting in the Urbach energy. As the Urbach energy indicates, a material's disorder level can influence the optical properties, from absorption and emission characteristics to charge carrier mobility. Understanding this can be crucial when designing optoelectronic devices or materials for specific light–matter interaction applications. The undefined values in ($\ln(\alpha)$) highlight the challenges of working with real-world data. The absorption might be so low in certain photon energy regions that obtaining meaningful logarithmic values is challenging. In such cases, data preprocessing or alternative analytical approaches might be necessary. The Urbach energies (E_U) for the different concentrations of By-pass in the composite, extracted from the slope of the linear fit to ($\ln(\alpha)$) *vs.* photon energy, are tabulated in Table 2.

The Urbach energy shows variations with different concentrations of By-pass. This suggests that the By-pass content influences the degree of disorder or structural imperfections in the composite. A higher Urbach energy indicates a greater degree of disorder. The Urbach energy provides insights into the local potential fluctuations in the material. These fluctuations can arise due to defects, impurities, or variations in bonding. The influence of By-pass concentration on (E_U) suggests that By-pass may introduce or modify these factors, leading to changes in the material's disorder. The Urbach energy and the resulting band tail states can influence various optical properties. These tail states can trap charge carriers, affecting processes like photoconductivity.

Moreover, understanding the material's disorder can provide insights into its radiation interaction characteristics for gamma attenuation applications. Materials with specific disorder levels might showcase different gamma interaction mechanisms or efficiencies. The ability to tune the Urbach energy by varying the By-pass concentration offers potential avenues to engineer the composite's optical properties for specific applications. One can optimize the composite's performance in optoelectronic devices or radiation shielding applications by controlling the degree of disorder.

As shown in Fig. 8, the Urbach energy varies across different concentrations of By-pass, indicating changes in the degree of disorder within the composite material. The concentration labeled "By-pass3" exhibits the highest Urbach energy, suggesting the highest degree of disorder among the samples. Conversely, "By-pass6" shows the lowest Urbach energy, indicating the least disorder. A higher Urbach energy represents a greater degree of disorder within the material. The disorder can arise from various sources, such as impurities, defects, or variations in crystallinity. The variations in Urbach energy with By-pass concentration implies that By-pass influences the structural or electronic characteristics of the composite. It could either introduce certain imperfections or counteract existing ones, leading to variations in disorder. A material's disorder level can influence its optical properties, charge carrier mobility, and interaction with radiation. As the Urbach energy indicates, understanding this disorder can be crucial for optimizing the composite's performance in specific applications, including gamma attenuation.

3.3. Radiation shielding properties

Fig. 9(a)–(e) shows a plot of the $\mathrm{Ln}(I/I_0)$ as a function of glass thickness for all the glasses studied at the various energies. According to what is shown in this figure, the $\mathrm{Ln}(I/I_0)$ values for By-pass0, By-pass3, By-pass6, By-pass10, and By-pass15 go up when there is an increasing photon energy. In addition, at the studied energies, the $\mathrm{Ln}(I/I_0)$ values decrease with increasing By-pass.

For example, at 662 keV $[\mathrm{Ln}(I/I_0)]_{\text{By-pass0}} > [\mathrm{Ln}(I/I_0)]_{\text{By-pass3}} > [\mathrm{Ln}(I/I_0)]_{\text{By-pass6}} > [\mathrm{Ln}(I/I_0)]_{\text{By-pass10}} > [\mathrm{Ln}(I/I_0)]_{\text{By-pass15}}$. At certain energy, for example, 80 keV, the $\mathrm{Ln}(I/I_0)$ values for all glasses decrease as a function of glass compression. −0.92, −0.93, −0.94, −0.95, and −0.97 are the $\mathrm{Ln}(I/I_0)$ values for By-pass0, By-pass3, By-pass6, By-pass10 and By-pass15 glasses, respectively (Fig. 10). This is because of the shift in density (D) that occurs while going from By-pass0 to By-pass3 to By-pass6 to By-pass10 to By-pass15. Moreover, the crystalline phases generated in By-pass15 are denser than those created

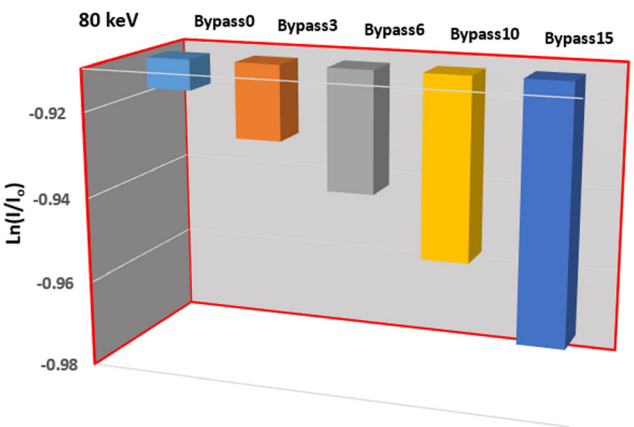

Fig. 10 ($\mathrm{Ln}(I/I_0)$) values against glass concentration at 80 keV.

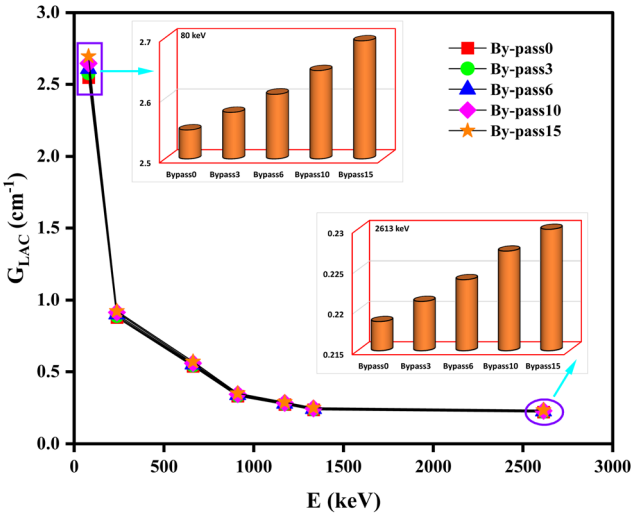

Fig. 11 Linear attenuation coefficient (G_{LAC}) against photon energy for all studied samples at selected photon energy.

in By-pass0, making the network structure more compact. The behavior of Ln(I/I_0) with energy and glass composition also indicates that the photon attenuation lowers with rising photon energy and rises with altering the amount of By-pass content. The slope of the Ln(I/I_0)-glass thickness graphs has been used to measure the G_{LAC} values for By-pass0, By-pass3, By-pass6, By-pass10, and By-pass15 glass samples at different energies.

The G_{LAC} values for each studied glass are shown in Fig. 11 at the chosen photon energy. As can be seen in this figure, the G_{LAC} values for all glass ceramics go down as the photon energy goes up. This might be because there are three different ways in which photons can impart energy to matter. Glasses interact with gamma rays through the photoelectric effect, Compton scattering, and pair creation at low, medium, and high photon energies.[43–46] When measured at a certain energy (inset figures for 80 and 2614 keV, Fig. 11), the G_{LAC} values increase as the percentage of By-pass increases. The glass with the smallest G_{LAC} values is By-pass0 ($20Na_2O–10Fe_2O_3–20Bi_2O_3–50P_2O_5$), while the glass with the largest G_{LAC} values is By-pass15 (15By-pass-$20Na_2O–10Fe_2O_3–20Bi_2O_3–35P_2O_5$). The mass attenuation coefficient (G_{MAC}) results for all glasses, measured using glass density and G_{LAC} values, have been plotted at 80, 662, 1173, and 2614 keV in Fig. 12. All results are listed in Table 3. This table indicates that the G_{MAC} behaviors with photon energy and sample concentration are identical to G_{LAC} behaviors for all glasses.[47–50]

The half-value layers, denoted by G_{HVL}, and the mean free path, denoted by G_{MFP}, have been computed with the help of the G_{LAC} values. The values of G_{HVL} and G_{MFP} for all the tested

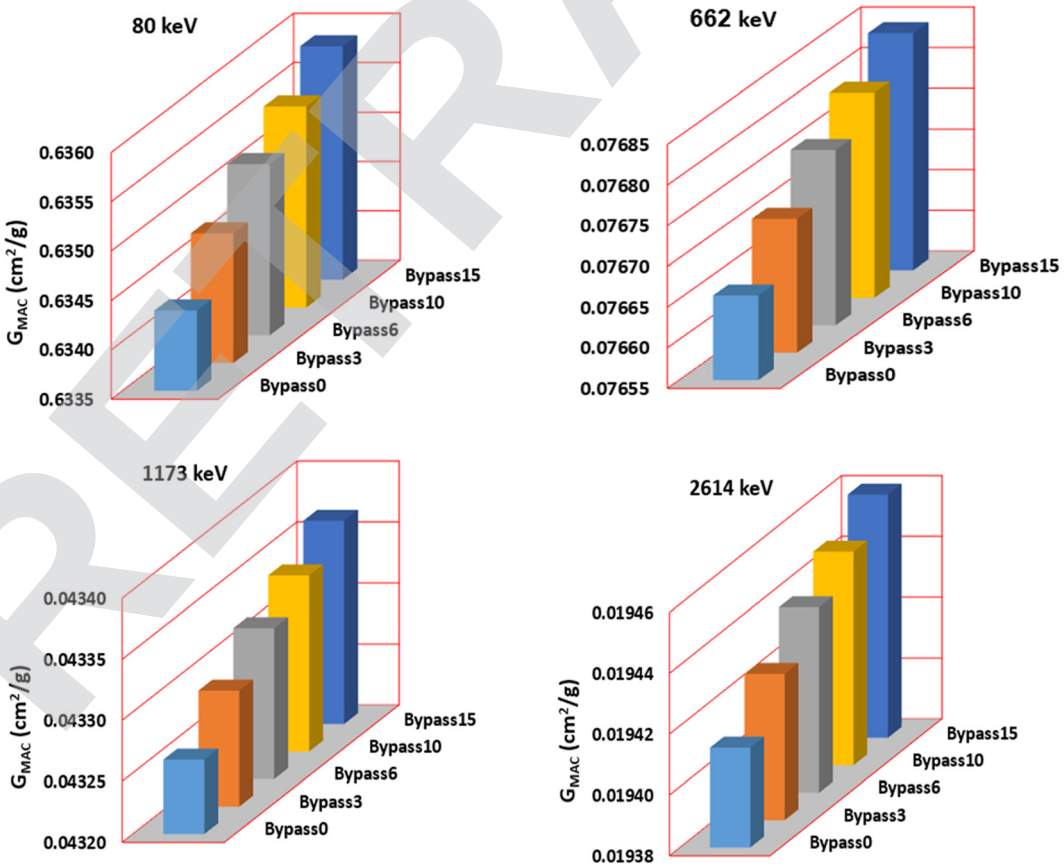

Fig. 12 Mass attenuation coefficient (G_{LAC}) against photon energy for all studied glasses at selected photon energy.

Table 3 Mass attenuation coefficient for all glasses at selected photon energy

Code	80 keV	238 keV	662 keV	911 keV	1173 keV	1333 keV	2614 keV
By-pass0	0.6343	0.2132	0.0767	0.0557	0.0433	0.0381	0.0194
By-pass3	0.6348	0.2134	0.0767	0.0557	0.0433	0.0381	0.0194
By-pass6	0.6352	0.2135	0.0768	0.0558	0.0433	0.0381	0.0194
By-pass10	0.6355	0.2136	0.0768	0.0558	0.0433	0.0381	0.0195
By-pass15	0.6359	0.2137	0.0768	0.0558	0.0434	0.0382	0.0195

glass samples are displayed in Fig. 13 and Fig. 14 at the chosen photon energy. As can be observed in these figures, the G_{HVL} and G_{MFP} values go up as the photon energy increases, but they go down when By-pass effects are considered. Compared to other glass samples, the By-pass15 sample, shown to have the maximum density among the glass ceramics researched, has the lowest G_{HVL} values at the tested photon energy.

Table 4 shows that the By-pass15 sample has the smallest G_{HVL} values, at 662, 1173, and 1333 keV, than S1,[51] S2,[52] S3,[53] PCNKBi7.5,[54] Pb20,[55] PbG,[56] S5[57] and different concretes (Ordinary concrete (OC), hematite-serpentine (HSC), ilmenite-limonite (ILC), basalt-magnetite (BMC), steel-scrap (SSC)).[58] Fig. 15 and 16 present a comprehensive analysis of the radiation protection efficiency (RPE) for glasses with varying By-pass content. Fig. 15 illustrates the RPE as a function of glass thickness across a spectrum of photon energies for each By-pass concentration. It is immediately apparent that the RPE improves with increasing glass thickness, which is consistent with the expected behavior of gamma radiation attenuation. Notably, this increase in RPE is more pronounced in glasses with higher By-pass content, indicating that By-pass plays a significant role in enhancing the shielding properties of the glass. Fig. 16 compares RPE at two specific photon energies, 80 keV and 2614 keV, for the different By-pass concentrations. At the lower energy of 80 keV, the RPE is substantially higher across all samples, which indicates the more effective interaction of low-energy photons with the glass matrix. The By-pass15 sample exhibits the highest RPE at this energy, reinforcing that the By-pass content correlates with improved attenuation.

Conversely, at the higher energy of 2614 keV, there is an overall reduction in RPE for all samples, which aligns with the decreased efficiency of gamma-ray attenuation at higher energies due to the predominance of less interactive processes such as pair production. However, even at this higher energy, the By-pass15 sample maintains a higher RPE than the By-pass0

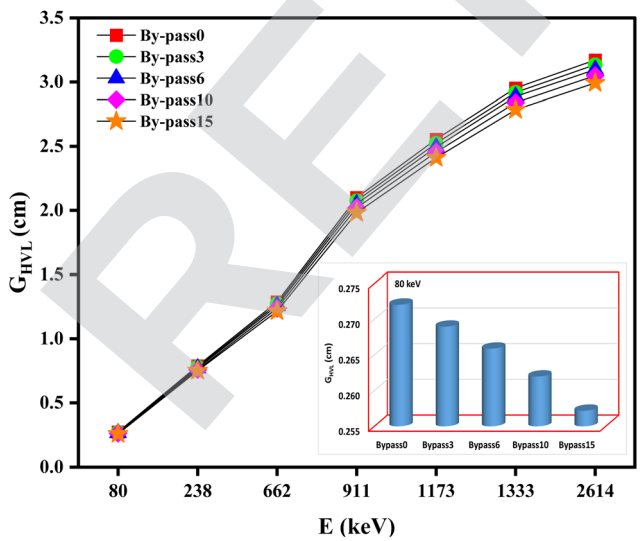

Fig. 13 Half value layer (G_{HVL}) against photon energy for all studied samples.

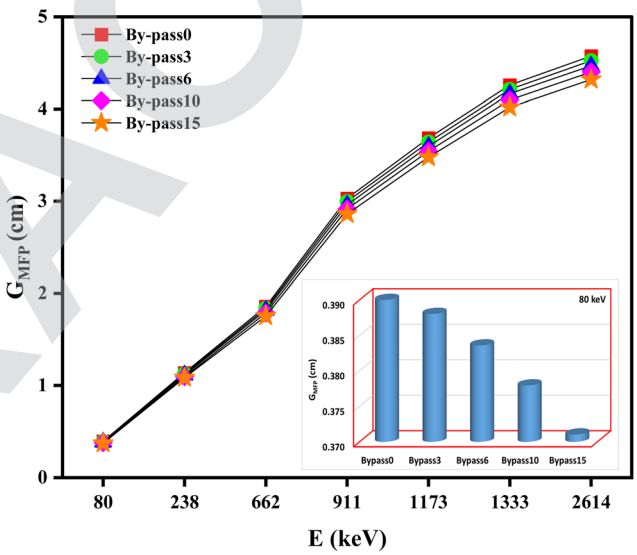

Fig. 14 Mean free path (G_{MFP}) against photon energy for all studied samples.

Table 4 Half value layer values of the By-pass15 glass sample compared to other glasses and concrete

	Half value layer (G_{HVL}) (cm)			
Glass	662 keV	1173 keV	1333 keV	Ref.
BBSDy	**1.22**	**2.41**	**2.78**	**This work**
S1	4.48	5.87	6.27	51
S2	3.80	4.99	5.32	52
S3	3.06	4.04	4.31	53
PCNKBi7.5	3.92	5.14	5.49	54
Pb20	3.85	5.13	5.48	55
PbG	3.77	4.95	5.28	56
S5	3.36	4.51	4.82	57
OC	3.80	4.98	5.31	58
HSC	3.62	4.75	5.07	
ILC	3.19	4.19	4.47	
BMC	2.98	3.91	4.17	
SSC	2.32	3.05	3.25	

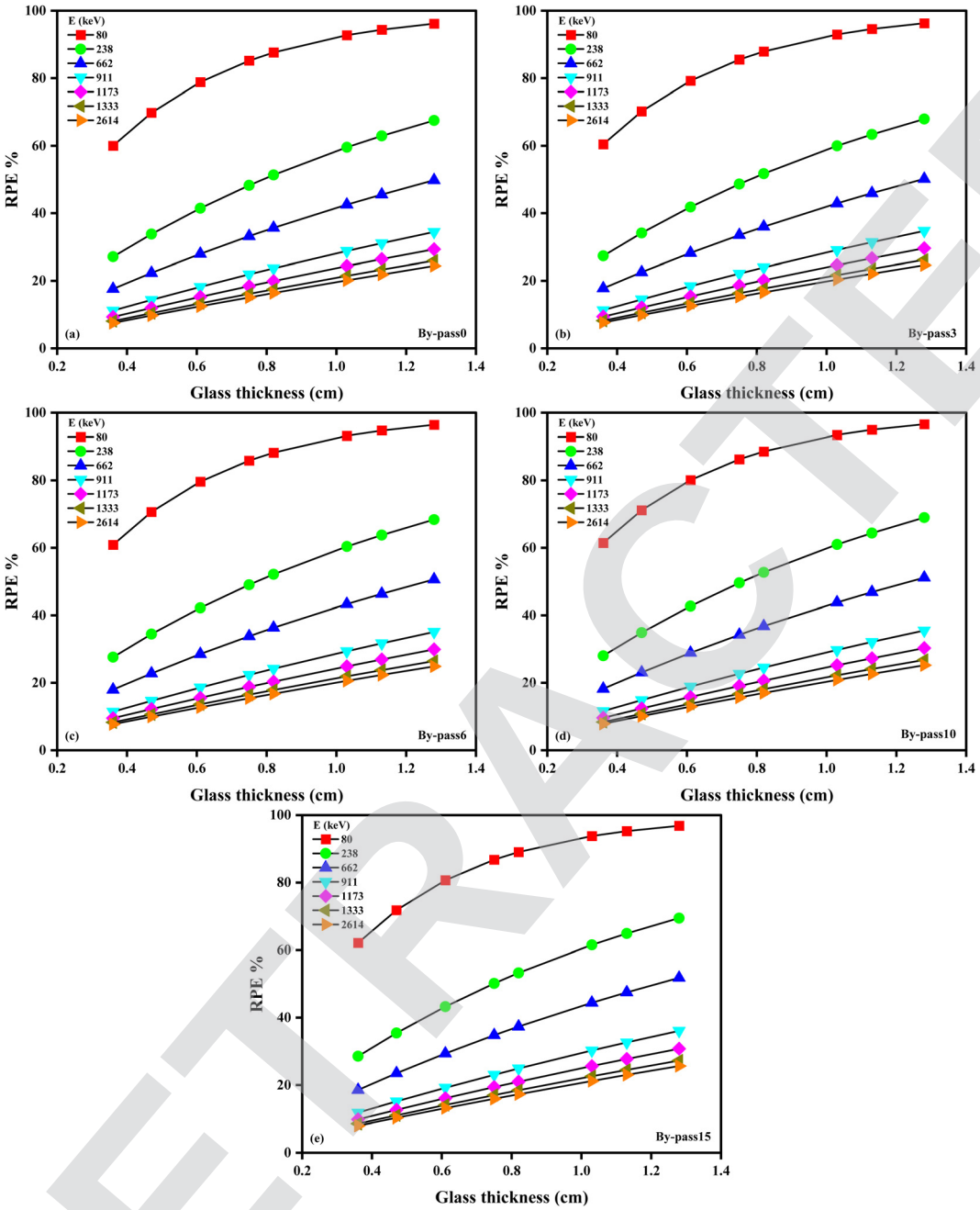

Fig. 15 (a)–(e) Radiation protection efficiency (RPE) for all studied samples at a selected photon energy.

sample, though the difference is less marked than at 80 keV. This trend confirms the beneficial addition of By-pass to the glass, which not only contributes to increased density but may also introduce structural variations that favor photon attenuation. The interplay between By-pass concentration and RPE is complex and reflects the intricate balance of multiple factors. The compositional variation affects the density and atomic number, critical parameters for gamma-ray shielding.[59–62] By-pass components such as silica (SiO_2) and alumina (Al_2O_3) provide additional electron density, which is beneficial for the photoelectric effect at lower energies, while the increase in the overall atomic number enhances the probability of Compton scattering. As the photon energy escalates, these effects become less pronounced, yet the compositional benefits of By-pass are still evident. The data across Fig. 15 and 16 showcase the significance of glass composition, particularly the By-pass content, in dictating the RPE. The consistent pattern reinforces our hypothesis that By-pass waste, when integrated into glass matrices, can significantly improve the material's ability to shield against gamma radiation, offering a dual benefit of waste utilization and enhanced protection against ionizing radiation.

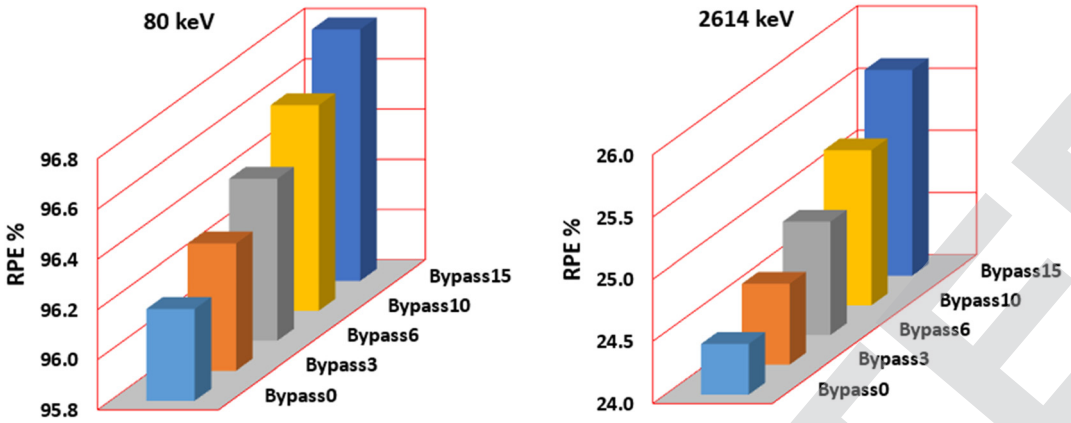

Fig. 16 Radiation protection efficiency (RPE) for all studied glasses at 80 and 2614 keV.

4. Conclusions

The results present insightful data that could revolutionize the application of such glasses in gamma shielding endeavors. The XRD patterns of the glass samples confirmed their amorphous nature, denoting a broad scope of potential applications. In the optical domain, UV-visible analysis indicated an absorption surge between 400 and 850 nm as the By-pass concentration increased. Specifically, the By-pass15 sample displayed superior absorption, suggesting the pronounced role of By-pass in enhancing the composite's absorption capacity. From the radiation shielding analysis, the By-pass15 sample outperformed its counterparts. The By-pass15 glass composition notably achieved the lowest half-value layer (G_{HVL}) measurements across the photon energies tested, with values at 662 keV, 1173 keV, and 1333 keV being lower than those of conventional materials like lead-based glass (Pb20 and PbG), indicating a superior radiation shielding capability. Furthermore, the radiation protection efficiency (RPE) of the By-pass15 glass showed a significant increase, outperforming the baseline By-pass0 composition by displaying RPE values that were consistently higher across all thicknesses, with the greatest differential observed at the lower photon energy of 80 keV. In light of these findings, the glasses, especially the By-pass15, emerge as potential game-changers in the domain of radiation shielding. Their amorphous nature, enhanced absorption capabilities, and superior shielding properties position them as strong contenders in gamma radiation protection. Future research can further optimize these materials, potentially paving the way for safer and more efficient environments in industries relying heavily on radioactive isotopes.

Data availability

The present authors declare that the work data and materials are available.

Conflicts of interest

The authors declare no competing interests.

References

1 G. Tyagi, A. Singhal, S. Routroy, D. Bhunia and M. Lahoti, A review on sustainable utilization of industrial wastes in radiation shielding concrete, *Mater. Today Proc.*, 2020, **32**, 746–751, DOI: **10.1016/J.MATPR.2020.03.474**.

2 A. M. Ali, S. A. M. Issa, H. Algarni, H. O. Tekin, H. M. H. Zakaly, M. A. Sayed and M. Rashad, Structural, surface morphology and radiation shielding properties of barium ferrite powder, *Physica Scripta*, 2021, **96**(9), 095805, DOI: **10.1088/1402-4896/ac03e0**.

3 M. Dobiszewska, O. Bagcal, A. Beycioğlu, D. Goulias, F. Köksal, B. Płomiński and H. Ürünveren, Utilization of rock dust as cement replacement in cement composites: An alternative approach to sustainable mortar and concrete productions, *J. Build. Eng.*, 2023, **69**, 106180, DOI: **10.1016/J.JOBE.2023.106180**.

4 S. A. M. Issa, A. W. Alrowaily, C. Oche, A. M. A. Henaish, M. M. A. Halaka, N. S. Alatawi and H. M. H. Zakaly, Unveiling the potentials of polyvinyl alcohol/manganese chloride nanocomposites films: A detailed examination of their structural, spectral, and radiation properties, *Mater. Today Commun.*, 2023, **37**, 107177, DOI: **10.1016/J.MTCOMM.2023.107177**.

5 A. S. Ali, S. A. M. Issa, H. M. H. Zakaly, M. Rashad, I. Khan, B. Zhang, K. Akiyama, S. Kubuki and H. O. Tekin, Municipal waste slag for dyes photocatalytic and metal recovery applications through structural analysis and experimental characterization, *Int. J. Energy Res.*, 2021, **45**, 17691–17708, DOI: **10.1002/er.6884**.

6 A. El-Denglawey, H. M. H. Zakaly, K. Alshammari, S. A. M. Issa, H. O. Tekin, W. S. AbuShanab and Y. B. Saddeek, Prediction of mechanical and radiation parameters of glasses with high Bi2O3 concentration, *Results Phys.*, 2021, **21**, 103839, DOI: **10.1016/j.rinp.2021.103839**.

7 P. W. Ladenson, L. E. Braverman, E. L. Mazzaferri, F. Brucker-Davis, D. S. Cooper, J. R. Garber, F. E. Wondisford, T. F. Davies, L. J. DeGroot, G. H. Daniels, D. S. Ross, B. D. Weintraub, I. D. Hay, S. Levis, J. C. Reynolds, J. Robbins, D. V. Becker, R. R. Cavalieri, H. R. Maxon,

K. McEllin and R. Moscicki, Comparison of Administration of Recombinant Human Thyrotropin with Withdrawal of Thyroid Hormone for Radioactive Iodine Scanning in Patients with Thyroid Carcinoma, *N. Engl. J. Med.*, 1997, **337**, 888–896, DOI: **10.1056/NEJM199709253371304**.

8 H. O. Tekin, G. ALMisned, Y. S. Rammah, E. M. Ahmed, F. T. Ali, D. Sen Baykal, W. Elshami, H. M. H. Zakaly, S. A. M. Issa, G. Kilic and A. Ene, Transmission factors, mechanical, and gamma ray attenuation properties of barium-phosphate-tungsten glasses: Incorporation impact of WO3, *Optik*, 2022, **267**, 169643, DOI: **10.1016/J.IJLEO.2022.169643**.

9 I. R. Miousse, K. R. Kutanzi and I. Koturbash, Effects of ionizing radiation on DNA methylation: from experimental biology to clinical applications, *Int. J. Radiat. Biol.*, 2017, **93**, 457–469, DOI: **10.1080/09553002.2017.1287454**.

10 Y. Al-Hadeethi, M. S. Al-Buriahi and M. I. Sayyed, Bioactive glasses and the impact of Si3N4 doping on the photon attenuation up to radiotherapy energies, *Ceram. Int.*, 2020, **46**, 5306–5314, DOI: **10.1016/j.ceramint.2019.10.281**.

11 S. A. M. Issa, H. M. H. Zakaly, M. Rashad, A. S. Ali and H. O. Tekin, Fabrication, optical, structural, and gamma-ray attenuation properties of novel slag-waste glasses as superior shields: An exploring journey for waste to glass transformation, *Optik*, 2022, **270**, 169999, DOI: **10.1016/J.IJLEO.2022.169999**.

12 G. Almisned, W. Elshami, S. A. M. Issa, G. Susoy, H. M. H. Zakaly, M. Algethami, Y. S. Rammah, A. Ene, S. A. Al-Ghamdi, A. A. Ibraheem and H. O. Tekin, Enhancement of gamma-ray shielding properties in cobalt-doped heavy metal borate glasses: The role of lanthanum oxide reinforcement, *Materials*, 2021, **14**, 7703, DOI: **10.3390/ma14247703**.

13 U. Perişanoğlu, F. I. El-Agawany, E. Kavaz, M. Al-Buriahi and Y. S. Rammah, Surveying of Na2O3–BaO–PbO–Nb2O5–SiO2–Al2O3 glass-ceramics system in terms of alpha, proton, neutron and gamma protection features by utilizing GEANT4 simulation codes, *Ceram. Int.*, 2020, **46**, 3190–3202, DOI: **10.1016/J.CERAMINT.2019.10.023**.

14 G. Susoy, E. E. A. Guclu, O. Kilicoglu, M. Kamislioglu, M. S. Al-Buriahi, M. M. Abuzaid and H. O. Tekin, The impact of Cr2O3 additive on nuclear radiation shielding properties of LiF–SrO–B2O3 glass system, *Mater. Chem. Phys.*, 2020, **242**, 122481, DOI: **10.1016/J.MATCHEMPHYS.2019.122481**.

15 H. M. H. Zakaly, I. M. Nabil, S. A. M. Issa, N. Almousa, Z. Y. Khattari and Y. S. Rammah, Probing the elasticity and radiation protection potential of neodymium(III) doped zinc and niobium tellurite glasses: An integrated simulated and applied physics perspective, *Mater. Today Commun.*, 2023, **37**, 107113, DOI: **10.1016/j.mtcomm.2023.107113**.

16 A. M. A. Mostafa, S. A. M. Issa and M. I. Sayyed, Gamma ray shielding properties of PbO-B2O3-P2O5 doped with WO3, *J. Alloys Compd.*, 2017, **708**, 294–300, DOI: **10.1016/j.jallcom.2017.02.303**.

17 S. A. M. Issa, M. I. Sayyed, A. M. A. Mostafa, G. Lakshminarayana and I. V. Kityk, Investigation of mechanical and radiation shielding features of heavy metal oxide based phosphate glasses for gamma radiation attenuation applications, *J. Mater. Sci. Mater. Electron.*, 2019, **30**, 12140–12151, DOI: **10.1007/S10854-019-01572-X/FIGURES/15**.

18 H. M. H. Zakaly, S. A. M. Issa, H. O. Tekin, A. Badawi, H. A. Saudi, A. M. A. Henaish and Y. S. Rammah, An experimental evaluation of CdO/PbO-B2O3 glasses containing neodymium oxide: Structure, electrical conductivity, and gamma-ray resistance, *Mater. Res. Bull.*, 2022, 111828, DOI: **10.1016/j.materresbull.2022.111828**.

19 B. Aktas, M. Albaskar, S. Yalcin and K. Dogru, Optical properties of soda-lime-silica glasses doped with peanut shell powder, *Arch. Mater. Sci. Eng.*, 2016, **82**, 57–61, DOI: **10.5604/01.3001.0009.7104**.

20 B. Çetin, Ş. Yalçin, B. Aktaş and M. Albaşkara, Investigation of radiation shielding properties of soda-lime-silica glasses doped with different food materials, *Acta Phys. Pol. A*, 2017, **132**, 988–990, DOI: **10.12693/APHYSPOLA.132.988**.

21 B. Aktas, M. Albaskara, S. Yalcin and K. Dogru, Optical properties of soda-lime-silica glasses doped with eggshell powder, *Acta Phys. Pol. A*, 2017, **132**, 442–444, DOI: **10.12693/APHYSPOLA.132.442**.

22 M. I. Sayyed, Radiation shielding characterization of a Yb:CaBTeX glass system as a function of TeO2 concentration, *Opt. Quantum Electron.*, 2024, **56**, 1–11, DOI: **10.1007/s11082-023-05951-x**.

23 M. Y. Hanfi, M. I. Sayyed, E. Lacomme, I. Akkurt and K. A. Mahmoud, The influence of MgO on the radiation protection and mechanical properties of tellurite glasses, *Nucl. Eng. Technol.*, 2021, **53**, 2000–2010, DOI: **10.1016/j.net.2020.12.012**.

24 A. H. Almuqrin and M. I. Abualsayed, Influence of WO3 content on gamma rays attenuation characteristics of phosphate glasses at low energy range, *Open Chem.*, 2023, **21**(1), 20220308, DOI: **10.1515/chem-2022-0308**.

25 M. I. Sayyed, Effect of WO3 on the attenuation parameters of TeO2–La2O3-WO3 glasses for radiation shielding application, *Radiat. Phys. Chem.*, 2024, **215**, 111319, DOI: **10.1016/j.radphyschem.2023.111319**.

26 A. I. Elazaka, H. M. H. Zakaly, S. A. M. Issa, M. Rashad, H. O. Tekin, H. A. Saudi, V. H. Gillette, T. T. Erguzel and A. G. Mostafa, New approach to removal of hazardous Bypass Cement Dust (BCD) from the environment: 20Na2O-20BaCl2-(60-x)B2O3-(x)BCD glass system and Optical, mechanical, structural and nuclear radiation shielding competences, *J. Hazard. Mater.*, 2021, **403**, 123738, DOI: **10.1016/j.jhazmat.2020.123738**.

27 H. M. H. Zakaly, H. A. Saudi, H. O. Tekin, M. Rashad, S. A. M. Issa, Y. S. Rammah, A. I. Elazaka, M. M. Hessien and A. Ene, Glass fabrication using ceramic and porcelain recycled waste and lithium niobate: physical, structural, optical and nuclear radiation attenuation properties, *J. Mater. Res. Technol.*, 2021, **15**, 4074–4085, DOI: **10.1016/J.JMRT.2021.09.138**.

28 Z. Ghouleh and Y. Shao, Turning municipal solid waste incineration into a cleaner cement production, *J. Clean. Prod.*, 2018, **195**, 268–279, DOI: **10.1016/j.jclepro.2018.05.209**.

29 G. ALMisned, D. Sen Baykal, G. Kilic, E. Ilik, E. Rabaa, G. Susoy, H. M. H. Zakaly, A. Ene and H. O. Tekin,

Comparative analysis on application conditions of indium (III) oxide-reinforced glasses in nuclear waste management and source transportation: A Monte Carlo simulation study, *Heliyon*, 2023, **9**(3), e14274, DOI: **10.1016/j.heliyon.2023.e14274**.

30 M. I. A. Abdel Maksoud, O. I. Sallam, S. M. Kassem, R. A. Fahim and A. S. Awed, Novel Strategy for Hazardous Cement Bypass Dust Removal: Structural, Optical and Nuclear Radiation Shielding Properties of CBD-Bismuth Borate Glass, *J. Inorg. Organomet. Polym. Mater.*, 2022, **32**, 3533–3545, DOI: **10.1007/s10904-022-02378-x**.

31 Y. B. Saddeek, G. Y. Mohamed, H. Shokry Hassan, A. M. A. Mostafa and G. Abd Elfadeel, Effect of gamma irradiation on the FTIR of cement kiln dust-bismuth borate glasses, *J. Non-Cryst. Solids*, 2015, **419**, 110–117, DOI: **10.1016/j.jnoncrysol.2015.03.021**.

32 C. Gautam, A. Madheshiya, A. Kumar Singh, K. Kishor Dey and M. Ghosh, Synthesis, optical and solid NMR studies of strontium titanate borosilicate glasses doped with TeO2, *Results Phys.*, 2020, **16**, 102914, DOI: **10.1016/J.RINP.2019.102914**.

33 A. Madheshiya, C. Gautam and S. Kumar, Synthesis, structural and X-ray absorption spectroscopy of (PbxBi1-x).TiO3 borosilicate glass and glass ceramics, *J. Asian Ceram. Soc.*, 2017, **5**, 276–283, DOI: **10.1016/J.JASCER.2017.05.003**.

34 N. A. Elthair, E. M. Mustafa, A. A. Elbadawi, N. A. Elthair, E. M. Mustafa and A. A. Elbadawi, The Electrical and Optical Properties of Zn0.5Li2xMg0.5-xFe2O4 Lithium Doped Nanoparticle Prepared by Coprecipitation Method, *Open J. Appl. Sci.*, 2020, **10**, 551–560, DOI: **10.4236/OJAPPS.2020.109039**.

35 M. K. Halimah, M. F. Faznny, M. N. Azlan and H. A. A. Sidek, Optical basicity and electronic polarizability of zinc borotellurite glass doped La3+ ions, *Results Phys.*, 2017, **7**, 581–589, DOI: **10.1016/J.RINP.2017.01.014**.

36 A. Kumar, R. Kaur, M. I. Sayyed, M. Rashad, M. Singh and A. M. Ali, Physical, structural, optical and gamma ray shielding behavior of (20 + x) PbO – 10 BaO – 10 Na2O – 10 MgO – (50-x) B2O3 glasses, *Phys. B*, 2019, **552**, 110–118, DOI: **10.1016/J.PHYSB.2018.10.001**.

37 M. Mazilu, N. Tigau and V. Musat, Optical properties of undoped and Al-doped ZnO nanostructures grown from aqueous solution on glass substrate, *Opt. Mater.*, 2012, **34**, 1833–1838, DOI: **10.1016/J.OPTMAT.2012.05.010**.

38 S. Yasmeen, F. Iqbal, T. Munawar, M. A. Nawaz, M. Asghar and A. Hussain, Synthesis, structural and optical analysis of surfactant assisted ZnO–NiO nanocomposites prepared by homogeneous precipitation method, *Ceram. Int.*, 2019, **45**, 17859–17873, DOI: **10.1016/J.CERAMINT.2019.06.001**.

39 M. A. Ditta, M. A. Farrukh, S. Ali and N. Younas, X-ray peak profiling, optical parameters and catalytic properties of pure and CdS doped ZnO–NiO nanocomposites, *Russ. J. Appl. Chem.*, 2017, **90**, 151–159, DOI: **10.1134/S1070427217010220/METRICS**.

40 A. S. Hassanien and A. A. Akl, Influence of composition on optical and dispersion parameters of thermally evaporated non-crystalline Cd50S50−xSex thin films, *J. Alloys Compd.*, 2015, **648**, 280–290, DOI: **10.1016/J.JALLCOM.2015.06.231**.

41 F. K. Shan and Y. S. Yu, Band gap energy of pure and Al-doped ZnO thin films, *J. Eur. Ceram. Soc.*, 2004, **24**, 1869–1872, DOI: **10.1016/S0955-2219(03)00490-4**.

42 F. Migliorini, S. Belmuso, R. Dondè, S. De Iuliis and I. Altman, To optical properties of carbon nanoparticles: A need in comprehending Urbach energy, *Carbon Trends*, 2022, **8**, 100184, DOI: **10.1016/J.CARTRE.2022.100184**.

43 H. M. H. Zakaly, D. E. Abulyazied, H. A. Saudi, B. M. Alotaibi and S. A. M. Issa, Surface hardness, thermal, optical, and photon attenuation coefficients assessment for dysprosium-doped tellurite glasses, *J. Rare Earths*, 2023, **41**, 1083–1090, DOI: **10.1016/J.JRE.2022.05.009**.

44 M. I. Sayyed, S. A. M. Issa and S. H. Auda, Assessment of radio-protective properties of some anti-inflammatory drugs, *Prog. Nucl. Energy*, 2017, **100**, 297–308, DOI: **10.1016/j.pnucene.2017.07.003**.

45 H. M. H. Zakaly, D. E. Abulyazied, S. A. M. Issa, A. W. Alrowaily, H. A. Saudi and H. M. Abomostafa, Optical, Microhardness, and Radiation Shielding Properties of Rare Earth Doped Strontium Barium Titanate Polyvinylidene Fluoride Nanocomposites, *J. Inorg. Organomet. Polym. Mater.*, 2023, **33**, 1177–1190, DOI: **10.1007/S10904-023-02564-5**.

46 H. M. H. Zakaly, H. O. Tekin, A. M. S. Issa, A. W. Alrowaily, A. Ene and Y. S. Rammah, Dual Impacts of Bi2O3/B2O3 Substitution on Mechanical and Attenuation Properties of Zinc–Bismuth–Borate Ternary Glasses for Diagnosis γ-Rays Shielding Materials Application, *J. Inorg. Organomet. Polym. Mater.*, 2023, **33**(6), 1495–1506, DOI: **10.1007/S10904-022-02527-2**.

47 A. S. Abouhaswa, H. M. H. Zakaly, S. A. M. Issa, M. Rashad, M. Pyshkina, H. O. Tekin, R. El-Mallawany and M. Y. A. Mostafa, Synthesis, physical, optical, mechanical, and radiation attenuation properties of TiO2–Na2O–Bi2O3–B2O3 glasses, *Ceram. Int.*, 2021, **47**, 185–204, DOI: **10.1016/j.ceramint.2020.08.122**.

48 G. Kilic, S. A. M. Issa, E. Ilik, O. Kilicoglu and H. O. Tekin, A journey for exploration of Eu2O3 reinforcement effect on zinc-borate glasses: Synthesis, optical, physical and nuclear radiation shielding properties, *Ceram. Int.*, 2020, **47**(2), 2572–2583, DOI: **10.1016/j.ceramint.2020.09.103**.

49 A. M. A. Mostafa, H. M. Zakaly, S. A. Al-Ghamdi, S. A. Issa, M. Al-Zaibani, R. M. Ramadan and E. F. El Agammy, PbO–Sb2O3–B2O3–CuO glassy system: Evaluation of optical, gamma and neutron shielding properties, *Mater. Chem. Phys.*, 2021, **258**, 123937, DOI: **10.1016/j.matchemphys.2020.123937**.

50 H. O. Tekin, G. ALMisned, H. M. H. Zakaly, A. Zamil, D. Khoucheich, G. Bilal, L. Al-Sammarraie, S. A. M. Issa, M. S. Al-Buriahi and A. Ene, Gamma, neutron, and heavy charged ion shielding properties of Er3 + -doped and Sm3 + -doped zinc borate glasses, *Open Chem.*, 2022, **20**, 130–145, DOI: **10.1515/CHEM-2022-0128**.

51 B. Aktas, S. Yalcin, K. Dogru, Z. Uzunoglu and D. Yilmaz, Structural and radiation shielding properties of chromium oxide doped borosilicate glass, *Radiat. Phys. Chem.*, 2019, **156**, 144–149, DOI: **10.1016/J.RADPHYSCHEM.2018.11.012**.

52 S. Yalcin, B. Aktas and D. Yilmaz, Radiation shielding properties of Cerium oxide and Erbium oxide doped obsidian glass, *Radiat. Phys. Chem.*, 2019, **160**, 83–88, DOI: 10.1016/J.RADPHYSCHEM.2019.03.024.

53 M. H. A. Mhareb, Y. S. M. Alajerami, M. I. Sayyed, N. Dwaikat, M. Alqahtani, F. Alshahri, N. Saleh, N. Alonizan, T. Ghrib and S. I. Al-Dhafar, Radiation shielding, structural, physical, and optical properties for a series of borosilicate glass, *J. Non-Cryst. Solids*, 2020, **550**, 120360, DOI: 10.1016/J.JNONCRYSOL.2020.120360.

54 H. A. Al-Yousef, M. I. Sayyed, M. Alotiby, A. Kumar, Y. S. Alghamdi, B. M. Alotaibi, N. A. M. Alsaif, K. A. Mahmoud and Y. Al-Hadeethi, Evaluation of optical, and radiation shielding features of New phosphate-based glass system, *Optik*, 2021, **242**, 167220, DOI: 10.1016/J.IJLEO.2021.167220.

55 A. H. Almuqrin, A. Kumar, J. F. M. Jecong, N. Al-Harbi, E. Hannachi and M. I. Sayyed, Li2O-K2O-B2O3-PbO glass system: Optical and gamma-ray shielding investigations, *Optik*, 2021, **247**, 167792, DOI: 10.1016/J.IJLEO.2021.167792.

56 F. F. Al-Harbi, N. S. Prabhu, M. I. Sayyed, A. H. Almuqrin, A. Kumar and S. D. Kamath, Evaluation of structural and gamma ray shielding competence of Li2O-K2O-B2O3-HMO (HMO = SrO/TeO2/PbO/Bi2O3) glass system, *Optik*, 2021, **248**, 168074, DOI: 10.1016/J.IJLEO.2021.168074.

57 S. Singh, R. Kaur, S. Rani and B. S. Sidhu, Physical, structural and nuclear radiation shielding behaviour of xBaO-(0.30-x)MgO-0.10Na2O-0.10Al2O3-0.50B2O3 glass matrix, *Mater. Chem. Phys.*, 2022, **276**, 125415, DOI: 10.1016/J.MATCHEMPHYS.2021.125415.

58 I. I. Bashter, Calculation of radiation attenuation coefficients for shielding concretes, *Ann. Nucl. Energy*, 1997, **24**, 1389–1401, DOI: 10.1016/S0306-4549(97)00003-0.

59 I. S. Mahmoud, S. A. M. Issa, H. M. H. Zakaly, H. A. Saudi, A. S. Ali, Y. B. Saddeek, T. Alharbi and H. O. Tekin, Material characterization of WO3/Bi2O3 substituted calcium-borosilicate glasses: Structural, physical, mechanical properties and gamma-ray resistance competencies, *J. Alloys Compd.*, 2021, **888**, 161419, DOI: 10.1016/j.jallcom.2021.161419.

60 A. M. Madbouly, O. I. Sallam, S. A. M. Issa, M. Rashad, A. Hamdy, H. O. Tekin and H. M. H. Zakaly, Experimental and FLUKA evaluation on structure and optical properties and γ-radiation shielding capacity of bismuth borophosphate glasses, *Prog. Nucl. Energy*, 2022, **148**, 104219, DOI: 10.1016/J.PNUCENE.2022.104219.

61 S. A. M. Issa, A. M. Almutairi, K. Albalawi, O. K. Dakhilallah, H. M. H. Zakaly, A. Ene, D. E. Abulyazied, S. M. Ahmed, R. A. Youness and M. A. Taha, Production of Hybrid Nanocomposites Based on Iron Waste Reinforced with Niobium Carbide/Granite Nanoparticles with Outstanding Strength and Wear Resistance for Use in Industrial Applications, *Nanomaterials*, 2023, **13**(3), 537, DOI: 10.3390/NANO13030537.

62 A. M. Abd-Elnaiem, H. A. Saudi, H. M. H. Zakaly, S. A. M. Issa and M. Rashad, The effect of composition and γ-irradiation on the Vickers hardness, structural and optical properties of xLiNbO3-25CaO-35PbO-(40-x) waste systems, *Ceram. Int.*, 2021, **47**, 18751–18760, DOI: 10.1016/j.ceramint.2021.03.210.